

See discussions, stats, and author profiles for this publication at: <https://www.researchgate.net/publication/262872826>

Single Layer Graphene as an Effective Mediator of the Metal-Support Interaction

ARTICLE *in* JOURNAL OF PHYSICAL CHEMISTRY LETTERS · JUNE 2014

Impact Factor: 7.46 · DOI: 10.1021/jz500425j

CITATIONS

3

READS

56

11 AUTHORS, INCLUDING:



[Won Hui DOH](#)

Institute for Basic Science

18 PUBLICATIONS 60 CITATIONS

[SEE PROFILE](#)



[Anna Sobieszek](#)

Maria Curie-Sklodowska University in Lublin

2 PUBLICATIONS 8 CITATIONS

[SEE PROFILE](#)



[Leszek Salamacha](#)

Maria Curie-Sklodowska University in Lublin

10 PUBLICATIONS 77 CITATIONS

[SEE PROFILE](#)



[Francois Le Normand](#)

University of Strasbourg

205 PUBLICATIONS 2,423 CITATIONS

[SEE PROFILE](#)

Single-Layer Graphene as an Effective Mediator of the Metal–Support Interaction

Wen Luo,[†] Won Hui Doh,[†] Yeuk T. Law,[†] Fitsum Aweke,[‡] Anna Ksiazek-Sobieszek,[§] Andrzej Sobieszek,[§] Leszek Salamacha,[§] Krzysztof Skrzypiec,[§] François Le Normand,[‡] Andrzej Machocki,[§] and Spyridon Zafeiratos*,[†]

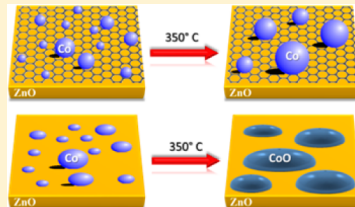
[†]Institut de Chimie et Procédés pour l'Energie, l'Environnement et la Santé (ICPEES), ECPM, UMR 7515 du CNRS, University of Strasbourg, 25 rue Becquerel Cedex 2, 67087 Strasbourg, France

[‡]ICube/MaCEPV, UMR 7357 of the University of Strasbourg and CNRS, rue du Loess, BP 20 CR, F-67087 Strasbourg Cedex 2, France

[§]University of Maria Curie-Sklodowska, Faculty of Chemistry, 3 Maria Curie-Sklodowska Square, PL 20-031, Lublin, Poland

S Supporting Information

ABSTRACT: Single-layer chemical vapor deposition (CVD)-grown graphene was transferred onto a ZnO (0001) substrate forming a large-area, low-defect density, protective layer. The quality of the graphene layer and its effect on the interaction between the ZnO support and vapor-deposited cobalt particles was investigated by spectroscopic and microscopic techniques. We demonstrate that the in-between graphene layer influences both the oxidation state and the morphology of cobalt upon annealing in vacuum. In particular, cobalt strongly interacts with the bare ZnO substrate forming flat particles, which are readily oxidized and redispersed upon annealing in ultrahigh vacuum conditions. In contrast, in the presence of the graphene interlayer, cobalt forms highly dispersed nanoparticles, which are resistant to oxidation, but prone to surface diffusion and agglomeration. The graphene layer exhibits remarkable stability upon cobalt deposition and vacuum annealing, while interaction with reactive gases can facilitate the formation of defects.



SECTION: Surfaces, Interfaces, Porous Materials, and Catalysis

Metal–support interaction, especially the metal–oxide interaction, has been studied for years since it plays a key role in many technologically important applications such as metal–oxide contacts in microelectronics and photovoltaic devices, gas sensors, and heterogeneous catalysis.^{1,2} It is generally accepted that the morphology and the electronic properties of supported overlayers are strongly influenced by the interaction with the substrate.^{3–5} Traditionally, supports like graphite, SiO₂, and Al₂O₃ are considered highly stable and relatively inert, while oxides such as TiO₂ and ZnO are known to have a strong influence on the structural and chemical characteristics of the deposited overlayer. In many applications, both the bulk (volume) and surface characteristics of the support are equally important. Bulk characteristics influence properties such as the mechanical stability, thermal and electric conductivity, photon absorption properties, and so on, while surface characteristics control the chemistry at the metal/support interface. For example, both the energy gap (bulk property) and the surface reactivity govern the performance of photocatalytic materials.⁶ In general, the surface and the bulk properties of supports are interconnected, and it is very difficult to modify one without influencing the other.

Graphene is considered as an attractive supporting material for metal clusters due to its unique electronic, structural, and chemical characteristics.^{7–14} In addition, graphene has been explored as an ultrathin barrier to protect different metals, such

as Cu,^{15,16} Cu/Ni,¹⁵ Ag,¹⁷ Fe,¹⁸ and so on, from corrosion in air, H₂O₂ and electrochemical environments. In all above studies, metals or relatively inert oxides were used as the supporting material of graphene layers. The effect of graphene on reactive oxide supports, which are known to interact actively with metal overlayers, has not been explored so far. In this work we demonstrate a new perspective of single-layer graphene as an interlayer that can dramatically influence the metal–support interaction. This is a potentially novel and stimulating application of graphene since it can act as a transparent, ultrathin, electron conductive, promoter/mediator of the substrate chemical properties.

Chemical vapor deposition (CVD)-grown single-layer graphene protected with a 0.5 μm thick poly methyl methacrylate (PMMA) was transferred onto the ultrahigh vacuum (UHV)-cleaned ZnO (0001) single crystal based on a slightly modified procedure previously reported by Suk et al.¹⁹ (Supporting Information 1). With this method, the continuity of the CVD-grown graphene can be preserved after transfer; however, impurities and defects can be introduced into graphene layer, while traces of the PMMA film might also reside.^{19–23} One should note here that after the transfer of the

Received: February 27, 2014

Accepted: May 9, 2014

Published: May 9, 2014

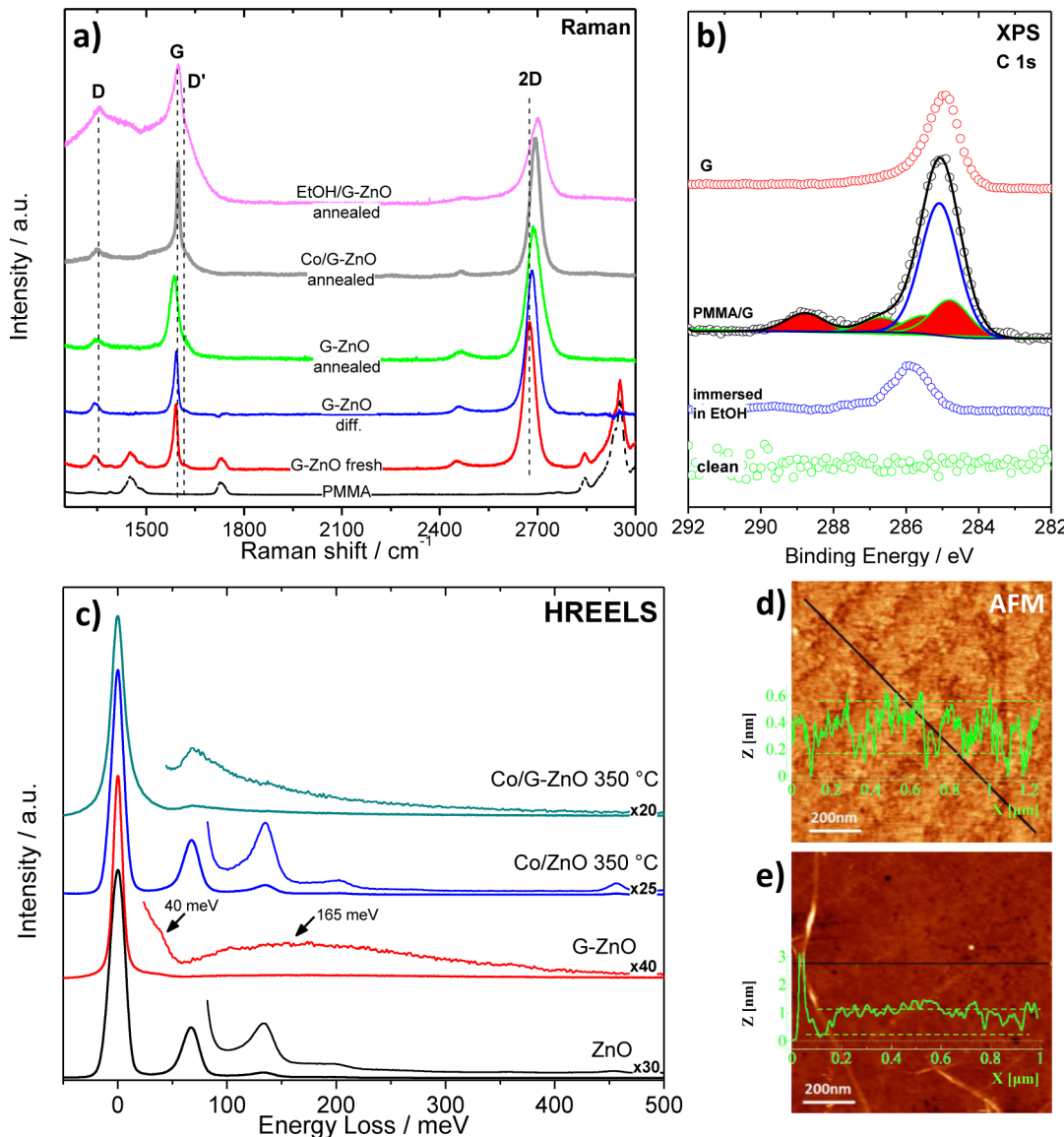


Figure 1. (a) Raman spectra of PMMA and G-ZnO samples before and after annealing as well as after cobalt deposition and ethanol exposure cycles, the blue line (G-ZnO diff.) derives after subtraction of PMMA to G-ZnO spectrum. (b) From bottom to top: XPS C 1s core level spectra of the clean bare ZnO (0001) substrate, after immersion in ethanol bath, after graphene transfer, after vacuum annealing. (c) From bottom to top: HREELS spectra of ZnO, G-ZnO, Co/ZnO, and Co/G-ZnO after annealing at 350 °C. (d) Tapping-mode AFM topographic images of clean bare ZnO and (e) G-ZnO samples. The line profiles along the lines depicted in the AFM images are superimposed in the figures.

PMMA/graphene layer on ZnO, the sample was annealed close to the PMMA glass transition temperature in order to increase the adhesion between graphene and ZnO and improve their contact.¹⁹ Despite this, areas where graphene does not lie flat but is curved forming a small gap with the ZnO substrate may still exist. Although in those areas graphene and ZnO are not in direct physical contact, graphene still acts as a separation barrier between ZnO and the metal overlayer.

Raman and X-ray photoelectron spectroscopy (XPS) C 1s results recorded after transferring the PMMA/graphene film onto ZnO and PMMA dissolution, abbreviated as G-ZnO, (Figure 1a,b, respectively) indicate spectral features due to traces of PMMA residues that were not totally removed by the ethanol treatment.^{24,25} Deconvolution of the C 1s XPS peak using previously described PMMA C 1s spectrum^{25,26} reveals that the residue PMMA signal is about 30% of the overall C 1s peak (in some transfer attempts, the residue PMMA signal

could reach up to 70%). This indicates that ethanol can effectively dissolve the majority of the PMMA layer, yet some PMMA residues remain after this procedure.^{22,27} Quantitative XPS calculations assuming the typical layer model²⁸ estimate the overall thickness of the carbon layer to be 1.5 ± 0.5 nm or roughly about 5 atomic layers (estimated carbon thickness 0.3 nm). For comparison, we immersed the bare ZnO crystal (without PMMA/graphene) into liquid ethanol, and we found that the signal of the C 1s peak due to residual species was 4 times lower, while the C 1s peak position was shifted to higher energies by about 1 eV (Figure 1b, second from bottom). This observation shows that graphene/PMMA can be clearly differentiated from residual carbon species in the C 1s spectrum. Annealing the sample at 350 °C in UHV for 1 h effectively removes the PMMA traces as indicated by the disappearance of the PMMA fingerprint peaks in both Raman and XPS spectra (Figure 1a,b). The thickness of the carbon

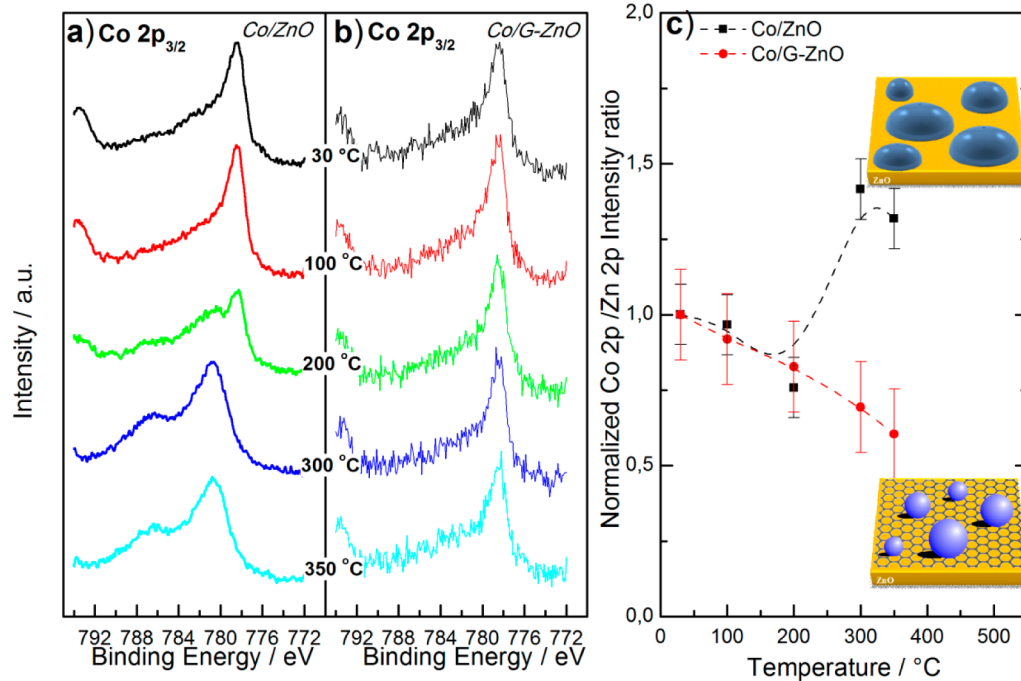


Figure 2. XPS spectra of (a) Co/ZnO and (b) Co/G-ZnO upon annealing at different temperatures. (c) Variation of the normalized XPS Co 2p/Zn 2p intensity ratios with temperature for Co/ZnO and Co/G-ZnO samples. To facilitate the comparison, the Co 2p/Zn 2p intensity ratio is normalized to the initial ratio at 30 °C. The error bars represent the data scattering as the deviation of the mean value obtained in three repeated experiments. A graphical representation of the cobalt particles' morphology after annealing at the higher temperature is included.

layer after annealing was estimated by XPS about 0.5 nm, compatible with the expected thickness of single-layer graphene.

The quality of the transferred graphene was characterized by Raman spectroscopy, which is an efficient method to conclude about the number of graphene sheets and their structural order.^{23,29–32} The main features of the Raman spectrum of graphene are the so-called G and 2D bands at about 1580 and 2700 cm⁻¹, respectively, while two additional bands around 1350 and 1610 eV (D and D' bands) are observed in disordered or defective graphene. The narrow symmetric 2D band and the relatively low G-to-2D band intensity ratio shown in Figure 1a can be used as a safe indicator of single-layer graphene.^{29,32} In addition, the low intensity of the D band (~1350 cm⁻¹) suggests that the graphene layer transferred on ZnO has a quite low defect density. Comparison of the Raman spectra of the G-ZnO sample before and after annealing in UHV shows that annealing has effectively removed the PMMA-related spectral features, without introducing new defects on the graphene layer (the D band remains small).

Surface phonons were examined using high-resolution energy-loss spectroscopy (HREELS). The clean ZnO (0001) surface (lower portion of Figure 1c) is characterized by surface optical phonons at 67, 134, and 200 meV due to long-range surface lattice vibrations.^{33,34} After transfer of the graphene layer and UHV annealing, the surface phonons of ZnO are completely screened. Instead, a weak shoulder at about 40 meV and a very broad structure centered at about 165 meV appeared (indicated by arrows in Figure 1c), similar to previous reports from graphene sheets on SiC.³⁵ The addition of graphene can influence the HREELS spectra in two ways: either by efficiently screening the ZnO substrate phonons or by inducing new features in the spectrum, for example due to the coupling of substrate phonons with plasmons from the graphene layer.³⁶

The inelastic mean free path (IMFP) of electrons with energy of 14 eV (the incident electron energy in our HREELS experiment) into carbon is about 0.02 nm.³⁷ This depth is significantly lower than the thickness of the graphene layer (about 0.35 nm) indicating that the ZnO substrate is not accessible to HREELS electrons. Full screening of the ZnO phonon features in the HREELS spectrum has been reported after deposition of thick metal overlayers on ZnO, e.g., 3 and 20 atomic layers for Pt³³ and Cu,³⁴ respectively. The presented HREELS spectra confirm the effective coverage of ZnO by graphene but cannot be conclusive about the effect of graphene on ZnO surface phonons. Overall, as compared to metals, single-layer graphene can be a very efficient, thermally stable material to screen the ZnO surface phonons.

The morphology of the sample surface was analyzed by atomic force microscopy (AFM). A typical AFM image and a line profile of the ZnO (0001) substrate after cleaning in UHV are shown in Figure 1d. The step-and-terrace structure can be observed with a step height of about 0.25 nm corresponding to a half lattice parameter of the unit cell of c₀.³⁸ In the AFM topographic image of the G-ZnO sample (Figure 1e), the layer is continuous and flat (root-mean-squared (RMS) roughness ~0.5 nm), although some wrinkles and small tears can be seen. As derived by the line profile curve superimposed in Figure 1e, the height of the graphene layer is about 1 nm compatible with a monolayer thickness for AFM measurements under atmospheric conditions.^{39,40} We should mention here that, although the theoretical thickness of single-layer graphene is 0.35 nm, the thickness of graphene in the AFM measurements can vary from 0.4 to 1 nm due to the chemical contrast between graphene and the substrate and the specific settings of the AFM instruments.^{41,42}

Cobalt, at coverage of 0.5 nm, or about 2 equiv layers, was evaporated onto annealed G-ZnO substrates in UHV at room

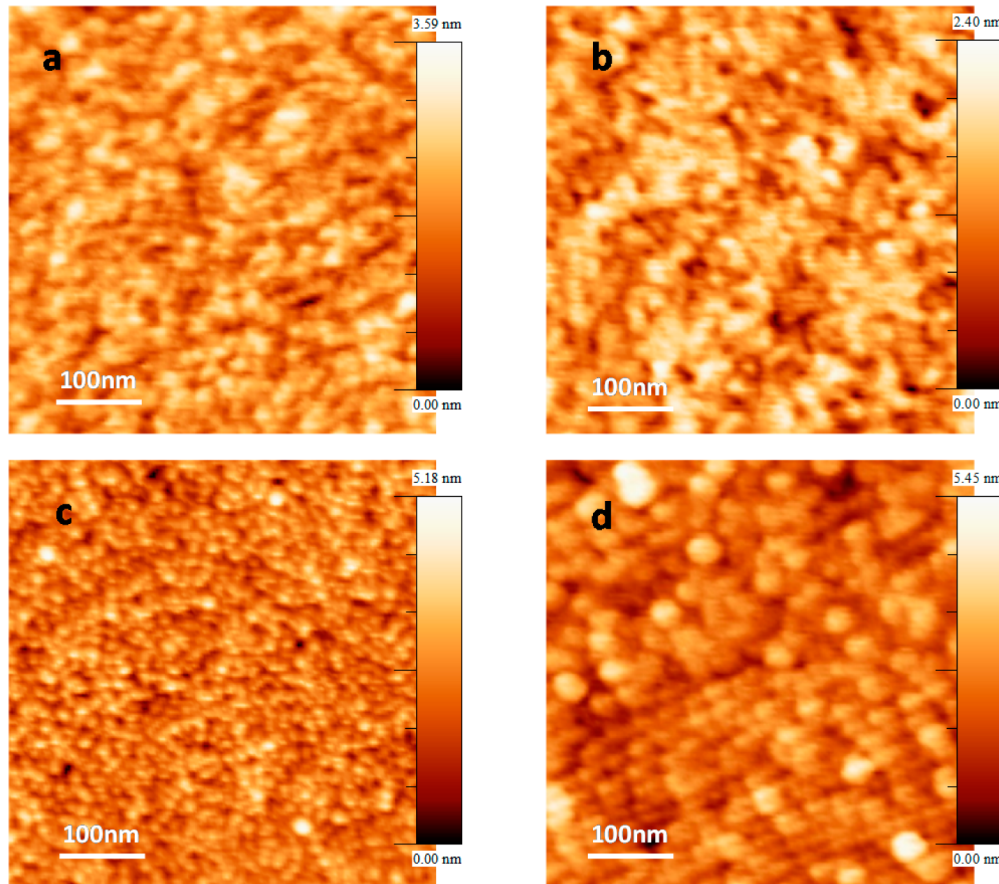


Figure 3. Tapping-mode AFM topographic images ($500 \times 500 \text{ nm}^2$) of (a) fresh Co/ZnO, (b) Co/ZnO after annealing at 350°C , (c) fresh Co/G-ZnO, and (d) Co/G-ZnO after annealing at 350°C .

temperature (abbreviated as Co/G-ZnO). For comparison, cobalt was also evaporated on a bare, clean ZnO substrate (abbreviated as Co/ZnO) under identical conditions (i.e., evaporation flux rate, duration and substrate temperature). Figure 2a,b compares the evolution of the Co 2p XPS peaks of Co deposited on ZnO and G-ZnO substrates as a function of the annealing temperature. Up to 100°C , the sharp Co 2p_{3/2} peak at 778.3 eV indicates the metallic Co state (Co^0)^{43,44} for both substrates. However, upon further annealing, the evolution of the Co 2p_{3/2} spectrum in the two substrates is considerably different. In particular, on bare ZnO, and starting from 200°C , the intensity of metallic Co 2p_{3/2} peak at 778.3 eV decreases and is gradually replaced by a component at 780.6 eV, which is typical for CoO^{43–45} (Figure 2a). It is interesting to note that, under the conditions examined, the oxidation is limited to CoO and does not proceed further to the more thermodynamically stable Co_3O_4 phase.⁴⁶ This result is in agreement with previous studies reporting that when Co/ZnO is annealed in vacuum, a solid state reaction takes place at the interface inducing cobalt oxidation.^{43,44,47} In contrast, annealing of the Co/G-ZnO sample does not cause any evident effect to the Co 2p_{3/2} peak shape, which remains identical to that of metallic Co even after annealing at 350°C . These results clearly show that the addition of graphene affects the metal–support interaction by preventing Co oxidation by ZnO. Apparently, the oxidation of Co by ZnO necessitates oxygen transport through a common interface between the two materials or substitution of Zn by Co ions in the ZnO oxide lattice. Defect-free graphene acts as a physical barrier for the in-diffusion of Co

while, as has been described previously, is it impermeable toward oxygen,^{48,49} which elucidates the observed resistance of Co to oxidation. This description accounts not only for areas that graphene is in physical contact with the support but also for curved graphene areas, since in both cases the Co–ZnO interaction is prohibited.

The XPS intensity ratio between Co 2p and Zn 2p photoelectron peaks ($I_{\text{Co}}/I_{\text{Zn}}$) is indicative of the cobalt dispersion on the substrate^{50,51} and as such, can be used to qualitatively report about the morphological changes of cobalt overlayer upon annealing. In Figure 2c, a plot of the normalized $I_{\text{Co}}/I_{\text{Zn}}$ is presented as a function of the annealing temperature for both Co/ZnO and Co/G-ZnO samples. Comparison of the $I_{\text{Co}}/I_{\text{Zn}}$ ratio in the two samples indicates very similar values up to 200°C , but significant deviation above this temperature. In particular, the decrease of $I_{\text{Co}}/I_{\text{Zn}}$ observed up to 200°C indicates that less Co but more ZnO substrate is exposed. This can be explained by Co particle agglomeration and/or by increase of their contact angle with the support. At temperatures higher than 200°C , the $I_{\text{Co}}/I_{\text{Zn}}$ ratio of the G-ZnO substrate continues to decrease monotonically, indicating that agglomeration carries on as the temperature increases. On the contrary, on bare ZnO the ratio increases above 200°C , showing redispersion of cobalt. It is evident that upon annealing the Co overlayer on bare ZnO, cobalt is oxidized to CoO and spreads out over the ZnO surface, while over G-ZnO agglomeration of cobalt is observed. The Co–Co cohesive energy and the Co–C dissociation energy are the key parameters that define the energetics of Co morphology on

Table 1. G band and 2D Band fwhm and Positions and the Intensity Ratios for G-ZnO under Various Treatments (Estimated Error $\pm 1.5 \text{ cm}^{-1}$)

sample	position G (cm^{-1})	G fwhm (cm^{-1})	position 2D (cm^{-1})	2D fwhm (cm^{-1})	intensity ratio $I_{\text{D}}/I_{\text{G}}$	intensity ratio $I_{\text{2D}}/I_{\text{G}}$
G-ZnO	1591	17	2676	44	0.15	2.26
G-ZnO annealed	1586	33	2689	58	0.10	1.72
Co/G-ZnO annealed	1598	11	2693	40	0.10	1.30
EtOH+G-ZnO annealed	1587	67	2698	43	0.64	0.49

G-ZnO. The Co–C dissociation energy has been reported to be about 155 kJ/mol,⁵² and the cohesive energy of Co in a bulk crystal is about 423 kJ/mol.⁵³ Considering the size, shape, and structure of the Co nanoparticles in our case, the Co–Co cohesive energy can be estimated to be around 395 kJ/mol (Supporting Information 2), which is much higher than the Co–C dissociation energy. Hence, at high temperatures where kinetic limitations are eliminated, diffusion across the G-ZnO surface and coalescence of cobalt particles is favored.

The surface morphology of the Co/ZnO and Co/G-ZnO samples before and after annealing was further studied by AFM. The surface of the fresh Co-ZnO sample (Figure 3a) is relatively flat and continuous, but becomes rougher than that of clean ZnO (Figure 1) and individual particles can be seen. After annealing Co-ZnO at 350 °C (Figure 3b) the surface of this sample becomes more flat, with an RMS roughness of 0.35 nm and an average height of 1.3 nm. We can even observe in this image that the CoO film follows the step-and-terrace structure of the ZnO (0001) substrate. As anticipated, the morphology of the Co deposit on the G-ZnO substrate is significantly different (Figure 3c). Co forms highly dispersed homogeneous particles on the G-ZnO surface, while after annealing, formation of larger Co aggregates is observed in the AFM image (Figure 3d), as is also deduced by the reduction of the $I_{\text{Co}}/I_{\text{Zn}}$ ratio in the XPS results.

In the HREELS spectrum recorded on Co/ZnO after annealing (Figure 1c), the loss features at 67 and 134 cm^{-1} due to ZnO substrate areas are clearly visible. In the presence of the graphene interlayer, after annealing, a very weak signal at about 70 meV coincides well with the more intense ZnO phonon and might come from uncovered ZnO areas within the grain boundaries of graphene nanocrystals. The minor contribution of this peak to the overall HREELS signal confirms the effective screening of ZnO phonon losses by graphene, even after cobalt deposition and annealing.

Having shown the important influence of graphene interlayer on the Co–ZnO interaction, we discuss the stability of the graphene layer upon UHV thermal treatment. As has been shown earlier, the frequency, the width, and the relative intensities of Raman peaks are sensitive to the strain, the number of defects, and the charge doping within the graphene layer.^{19,22,29,54,55} In Figure 1a, the Raman spectra of G-ZnO and Co/G-ZnO samples after annealing at 350 °C are shown. In addition, the position and the full width at half-maximum (fwhm) of the G and 2D bands are summarized in Table 1, along with the intensity ratios between the main Raman bands. The $I_{\text{D}}/I_{\text{G}}$ band intensity ratio has been used to estimate the defect density of the graphene layer.⁵⁴ This includes both the grain boundaries between the graphene nanocrystallites and the point-like defects. In general, higher $I_{\text{D}}/I_{\text{G}}$ ratios are indicative of higher degree of defects. The relatively low $I_{\text{D}}/I_{\text{G}}$ ratios before and after annealing shown in Table 1, suggest a low defect density that is not significantly affected by the cobalt deposition and the heating treatment. Casiraghi and co-workers

recently presented a method to distinguish the nature of defects in graphene by Raman spectroscopy.⁵⁶ They found that the intensity ratio of D and D' peaks changes from ca. 7 for vacancy-like defects to around 3.5 for boundary-like defects. As is evident from Figure 1a, the D to D' peak intensity ratio in this study is about 1. This indicates that the graphene defects are mainly associated with the boundaries in the graphene layer, possibly due to the different thermal expansion coefficients between graphene and ZnO. However, we should note that the graphene films used in the study of Casiraghi et al.⁵⁶ had defect density significantly higher than this work, which produced a clearly resolved D' peak. In our case, the D' peak appears as a small shoulder of the G peak, which hinders the analysis and demands more detailed studies on the nature of the defects.

Apart from the defects, Raman peaks can be informative about the mechanical strain within the graphene nanocrystallites. It has been proposed that mechanical strain induces a larger Raman shift of the 2D peak compared to that of the G band, followed by increase in the peak's fwhm.³⁰ On the basis of this argument and of the information presented in Table 1, we can deduce that annealing at 350 °C induces more strain within graphene as compared to the fresh G-ZnO sample. Indeed, the relative position of the 2D and G peaks is enlarged by 19 cm^{-1} , while the 2D peak fwhm becomes broader than that of the fresh G-ZnO sample by 30% (Supporting Information 3). Although defects and strain phenomena are usually interconnected,⁵⁷ we propose that the interaction between the graphene layer and ZnO is accountable for the observed strain since, as mentioned above, the defect density remains the same.

In the case of Co/G-ZnO, the Raman spectrum is characterized by an upshift in the G position and a significant decrease of its fwhm. In addition, the $I_{\text{2D}}/I_{\text{G}}$ ratio is further decreased. Previous studies have shown that such spectral modifications are induced by the electrical doping of graphene.^{22,58} The type of doping can be determined from the relative shifts between the G and 2D bands. In particular, the upshift of the G band position and the downshift of the 2D band indicates n-doping of graphene, whereas the upshift of both G and 2D bands implies p-doping.⁵⁹ As shown in Table 1, both the G and the 2D bands upshift compared to G-ZnO sample, suggesting an electron withdrawn from graphene toward the cobalt adlayer and therefore p-type (hole) doped graphene. Of course one cannot exclude the possibility of charge transfer interaction with the ZnO support, catalyzed by the presence of the cobalt overlayer. It is interesting to note here that our observation is in accordance with previous studies reporting that when gold nanoparticles are attached on graphene, there is electron charge transfer from graphene to the Au particles.^{8,60} Although Co and Au have evident differences in their reactivity, their resemblances in accepting electronic charge from graphene might serve as an interesting trend of the metal–graphene interaction.

Recently it was suggested that, apart from Raman spectra, the C 1s binding energy shifts can be used in order to evaluate charge transfer phenomena between graphene and substrate or overlayer structures.^{14,61,62} However, here we did not observe any binding energy shift in the C 1s spectra of graphene before and after cobalt deposition and annealing (the spectra were identical within the experimental error of ± 0.1 eV). There are two possible reasons that can explain the stability of the C 1s binding energy in our work. First, it is likely that the charge doping of cobalt in graphene is lower, compared to the other cases and therefore the shift of C 1s peak is much smaller and difficult to observe. According to Dahal et al.⁶¹ the C 1s core level shift of graphene in contact with a metal is correlated with the work function of the metal. In particular, graphene doping from metals with work function around 5 eV is limited and do not induce any binding energy shift to the C 1s peak. This can explain the absence of the C 1s binding energy shift in our case, since the work function of cobalt is reported to be around 5 eV.⁶³ Another possible reason is the influence of the final state effects on the binding energy shifts. We recall that the binding energy measured in a photoemission experiment does not directly reflect the state of the atom before photoemission (initial state), but is also affected by the redistribution of all surrounding electrons after photoemission in order to screen the core hole (final state effects). The effectiveness of the core hole screening depends not only on the particular element (intra-atomic screening), but also on the surrounding environment, i.e., atom co-ordination number and interaction with the support (extra-atomic screening). Therefore, it is possible that the magnitude of the C 1s peak shift upon doping is influenced by differences in the final state effects among different systems, and might be not a safe indicator of the charge doping.

The stability of graphene layer on ZnO was also tested upon ethanol exposure/desorption cycles in the UHV chamber (see Supporting Information 1 for experimental details). The Raman spectra recorded after three repeated ethanol exposure/desorption cycles show significant increase of the I_D/I_G intensity ratio along with a considerable broadening of the G and D bands (see Figure 1a and Table 1). Similar Raman spectra features have been recently ascribed to significant structural disorder of graphene due to the formation of defects.⁶⁴ In the optical microscopy (OM) images (Supporting Information 4), it can be seen that the initially intact graphene layer was fragmented in smaller graphene flakes of 5 to 20 μm size after ethanol exposure. In addition, micro-Raman measurements in points with different OM image contrast confirm the presence of microboundaries, where the ZnO substrate is not covered by graphene. The micro-Raman results are also supported by the decrease of the C 1s to Zn 2p signal ratio after ethanol exposure (Supporting Information 4). This is a quite remarkable result, since graphene is generally considered to be chemically inert to the interaction with gases. In addition, liquid ethanol was used for the removal of the PMMA layer without producing significant defect density (see OM image of the UHV annealed sample in Supporting Information 4). This indicates that during the desorption cycles ethanol reacts with graphene, possibly with dangling carbon bonds at the edge/boundaries of graphene introducing defects.

The results presented above can inspire new strategies to control the metal–support interaction in applications where the surface modification without the influence of the bulk characteristics of a material is required. This can be directly applicable in heterogeneous catalytic reactions where strong

interaction between the active phase and the support has been blamed for the catalysts' deactivation. For example, cobalt on oxide supports is used in two industrially relevant reactions, namely, the carbonylation of glycerol and the Fischer–Tropsch process. In both cases, strong metal support interaction induces formation of mixed cobalt-support oxides, which are difficult to reduce and cause irreversible deactivation.^{65,66} Using a model system we show here that graphene can prevent diffusion phenomena at the metal/oxide interface upon thermal treatment and eventually suppresses metal oxidation. Apparently, in industrial applications, easily scalable preparation methods of the graphene/oxide interface should be used, like, for example, via graphene oxide precursors,⁶⁷ while the stability of graphene under reaction conditions should be improved. However, cobalt/graphene and graphene/ZnO composite materials are already investigated for optoelectronic, photocatalytic, electrochemical and many other applications. In general, we believe that the results presented here do not concern only the particular Co–ZnO interface, but might be of broad interest in applications where metal–oxide or oxide–graphene interfaces play a key role.

Summarizing, in this work we transferred CVD-grown single-layer graphene onto ZnO(0001) and subsequently deposited Co in order to investigate the effect of graphene interlayer on the Co–ZnO interaction. It is shown that graphene could effectively prevent the oxidation of Co by the ZnO support and decrease cobalt dispersion. Raman results indicated an increase of graphene layer strain upon annealing and p-type doping upon Co deposition, but relatively low defect density.

EXPERIMENTAL METHODS

CVD-grown single-layer graphene (Trivial Transfer Graphene, $1 \times 1 \text{ cm}^2$, ACS material) was transferred onto the UHV-cleaned ZnO (0001) single crystal in atmosphere based on a slightly modified procedure previously reported by Suk et al.¹⁹ The residual PMMA was further cleaned by annealing in UHV at 350 °C for 1 h, and the cleanliness of the sample was verified by XPS and Raman. One-side polished polar ZnO(0001) single crystal ($10 \times 10 \times 0.33 \text{ mm}^3$, Crystec) was used as substrate. Prior to graphene transfer, the ZnO was cleaned under vacuum by following a standard procedure. Cobalt was evaporated under UHV on clean ZnO and graphene–ZnO substrates, using commercial e-beam evaporators. Raman spectra were recorded at room temperature and at atmospheric conditions by a Horiba spectrometer LabRam. The morphology of the samples was investigated at ambient conditions using a with NanoScope V (Bruker-Veeco) atomic force microscope. XPS and HREELS experiments were conducted in two UHV chambers, equipped with hemispherical electron analysers and a dual anode X-ray source and standard surface preparation facilities (ion sputter gun, LEED optics etc.).⁴³ In one of the UHV setups (VG Microtec, Strasbourg), the analysis area of the samples was maximized (ca. $8 \times 8 \text{ mm}^2$) in order to obtain representative information on large spatial area of the sample.

ASSOCIATED CONTENT

S Supporting Information

Detailed experimental part, calculation of the Co–Co cohesive energy, details of the 2D band Raman spectra, optical microscopy images, and the evolution of the XPS C 1s to Zn 2p intensity ratio. This material is available free of charge via the Internet at <http://pubs.acs.org>.

AUTHOR INFORMATION

Corresponding Author

*E-mail: spiros.zafeiratos@unistra.fr.

Notes

The authors declare no competing financial interest.

ACKNOWLEDGMENTS

The authors acknowledge support from Campus France, PHC Polonium, Project No. 27700SJ. Polish authors acknowledge funding from the Ministry of Science and Higher Education of Poland. W.L. would like to thank the China Scholarship Council (CSC) for the Ph.D. grant during his stay at the ICPEES. We also thank F. Antoni and R. Keller for their support during the Raman measurements.

REFERENCES

- (1) Comotti, M.; Li, W. C.; Spliethoff, B.; Schuth, F. Support Effect in High Activity Gold Catalysts for Co Oxidation. *J. Am. Chem. Soc.* **2006**, *128*, 917–924.
- (2) Einax, M.; Dieterich, W.; Maass, P. Colloquium: Cluster Growth on Surfaces: Densities, Size Distributions, and Morphologies. *Rev. Mod. Phys.* **2013**, *85*, 921–939.
- (3) Stakheev, A. Y.; Kustov, L. M. Effects of the Support on the Morphology and Electronic Properties of Supported Metal Clusters: Modern Concepts and Progress in 1990s. *Appl. Catal., A* **1999**, *188*, 3–35.
- (4) Zhou, W. P.; Yang, X.; Vukmirovic, M. B.; Koel, B. E.; Jiao, J.; Peng, G.; Mavrikakis, M.; Adzic, R. R. Improving Electrocatalysts for O₂ Reduction by Fine-Tuning the Pt-Support Interaction: Pt Monolayer on the Surfaces of a Pd₃Fe(111) Single-Crystal Alloy. *J. Am. Chem. Soc.* **2009**, *131*, 12755–12762.
- (5) Fujitani, T.; Nakamura, J. The Chemical Modification Seen in the Cu/ZnO Methanol Synthesis Catalysts. *Appl. Catal., A* **2000**, *191*, 111–129.
- (6) Kanan, D. K.; Carter, E. A. Band Gap Engineering of MnO Via ZnO Alloying: A Potential New Visible-Light Photocatalyst. *J. Phys. Chem. C* **2012**, *116*, 9876–9887.
- (7) Zhou, H.; Qui, C.; Liu, Z.; Yang, H.; Hu, L.; Li, J.; Yang, H.; Gu, C.; Sun, L. Thickness-Dependent Morphologies of Gold on N-Layer Graphenes. *J. Am. Chem. Soc.* **2010**, *132*, 944–946.
- (8) Liu, L.; Chen, Z.; Wang, L.; Polyakova, E.; Taniguchi, T.; Watanabe, K.; Hone, J.; Flynn, G. W.; Brus, L. E. Slow Gold Adatom Diffusion on Graphene: Effect of Silicon Dioxide and Hexagonal Boron Nitride Substrates. *J. Phys. Chem. B* **2013**, *117*, 4305–4312.
- (9) Zhou, Z.; Gao, F.; Goodman, D. W. Deposition of Metal Clusters on Single-Layer Graphene/Ru(0001): Factors That Govern Cluster Growth. *Surf. Sci.* **2010**, *604*, L31–L38.
- (10) Kamat, P. V. Graphene-Based Nanoarchitectures. Anchoring Semiconductor and Metal Nanoparticles on a Two-Dimensional Carbon Support. *J. Phys. Chem. Lett.* **2010**, *1*, 520–527.
- (11) Sutter, E.; Albrecht, P.; Wang, B.; Bocquet, M.-L.; Wu, L.; Zhu, Y.; Sutter, P. Arrays of Ru Nanoclusters with Narrow Size Distribution Templated by Monolayer Graphene on Ru. *Surf. Sci.* **2011**, *605*, 1676–1684.
- (12) Wintterlin, J.; Bocquet, M.-L. Graphene on Metal Surfaces. *Surf. Sci.* **2009**, *603*, 1841–1852.
- (13) Sutter, E.; Wang, B.; Albrecht, P.; Lahiri, J.; Bocquet, M.-L.; Sutter, P. Templating of Arrays of Ru Nanoclusters by Monolayer Graphene/Ru Moirés with Different Periodicities. *J. Phys.: Condens. Matter* **2012**, *24*, 314201.
- (14) Coy-Diaz, H.; Addou, R.; Batzill, M. Interface between Graphene and SrTiO₃(001) Investigated by Scanning Tunneling Microscopy and Photoemission. *J. Phys. Chem. C* **2013**, *117*, 21006–21013.
- (15) Chen, S.; Brown, L.; Levendorf, M.; Cai, W.; Ju, S.-Y.; Edgeworth, J.; Li, X.; Magnuson, C. W.; Velamakanni, A.; Piner, R. D.; et al. Oxidation Resistance of Graphene-Coated Cu and Cu/Ni Alloy. *ACS Nano* **2011**, *5*, 1321–1327.
- (16) Raman, R. K. S.; Banerjee, P. C.; Lobo, D. E.; Gullapalli, H.; Sumandasa, M.; Kumar, A.; Choudhary, L.; Tkacz, R.; Ajayan, P. M.; Majumder, M. Protecting Copper from Electrochemical Degradation by Graphene Coating. *Carbon* **2012**, *50*, 4040–4045.
- (17) Zhao, Y.; Xie, Y.; Hui, Y. Y.; Tang, L.; Jie, W.; Jiang, Y.; Xu, L.; Lau, S. P.; Chai, Y. Highly Impermeable and Transparent Graphene as an Ultra-Thin Protection Barrier for Ag Thin Films. *J. Mater. Chem. C* **2013**, *1*, 4956–4961.
- (18) Kang, D.; Kwon, J. Y.; Cho, H.; Sim, J.-H.; Hwang, H. S.; Kim, C. S.; Kim, Y. J.; Ruoff, R. S.; Shin, H. S. Oxidation Resistance of Iron and Copper Foils Coated with Reduced Graphene Oxide Multilayers. *ACS Nano* **2012**, *6*, 7763–7769.
- (19) Suk, J. W.; Kitt, A.; Magnuson, C. W.; Hao, Y. F.; Ahmed, S.; An, J. H.; Swan, A. K.; Goldberg, B. B.; Ruoff, R. S. Transfer of CVD-Grown Monolayer Graphene onto Arbitrary Substrates. *ACS Nano* **2011**, *5*, 6916–6924.
- (20) Reina, A.; Jia, X.; Ho, J.; Nezich, D.; Son, H.; Bulovic, V.; Dresselhaus, M. S.; Kong, J. Large Area, Few-Layer Graphene Films on Arbitrary Substrates by Chemical Vapor Deposition. *Nano Lett.* **2008**, *9*, 30–35.
- (21) Pirkle, A.; Chan, J.; Venugopal, A.; Hinojos, D.; Magnuson, C. W. The Effect of Chemical Residues on the Physical and Electrical Properties of Chemical Vapor Deposited Graphene Transferred to SiO₂. *Appl. Phys. Lett.* **2011**, *99*, 122108.
- (22) Lin, Y.-C.; Lu, C.-C.; Yeh, C.-H.; Jin, C.; Suenaga, K.; Chiu, P.-W. Graphene Annealing: How Clean Can it Be? *Nano Lett.* **2012**, *12*, 414–419.
- (23) Suzuki, S.; Orofeo, C. M.; Wang, S. M.; Maeda, F.; Takamura, M.; Hibino, H. Structural Instability of Transferred Graphene Grown by Chemical Vapor Deposition against Heating. *J. Phys. Chem. C* **2013**, *117*, 22123–22130.
- (24) Thomas, K. J.; Sheeba, M.; Nampoori, V. P. N.; Vallabhan, C. P. G.; Radhakrishnan, P. Raman Spectra of Polymethyl Methacrylate Optical Fibres Excited by a 532 nm Diode Pumped Solid State Laser. *J. Opt. A: Pure Appl. Opt.* **2008**, *10*, 055303.
- (25) Babanov, Y. A.; Nemtsova, O. M.; Kamensky, I. Y.; Mikhailova, S. S. The Determination of the True Profile of XPS Line by Regularization Method: I. Mathematical Algorithm and Numerical Simulations. *J. Electron Spectrosc. Relat. Phenom.* **2010**, *182*, 90–96.
- (26) Fulghum, J. E. Recent Developments in High Energy and Spatial Resolution Analysis of Polymers by XPS. *J. Electron Spectrosc. Relat. Phenom.* **1999**, *100*, 331–355.
- (27) Nathawat, R.; Kumar, A.; Acharya, N. K.; Vijay, Y. K. XPS and AFM Surface Study of PMMA Irradiated by Electron Beam. *Surf. Coat. Technol.* **2009**, *203*, 2600–2604.
- (28) Briggs, D.; Seah, P. *Practical Surface Analysis: Auger and X-ray Photoelectron Spectroscopy*; Wiley-VCH: Weinheim, Germany, 1990.
- (29) Casiraghi, C.; Pisana, S.; Novoselov, K. S.; Geim, A. K.; Ferrari, A. C. Raman Fingerprint of Charged Impurities in Graphene. *Appl. Phys. Lett.* **2007**, *91*, 233108.
- (30) Ni, Z.; Wang, Y.; Yu, T.; Shen, Z. Raman Spectroscopy and Imaging of Graphene. *Nano Res.* **2008**, *1*, 273–291.
- (31) Machado, B. F.; Serp, P. Graphene-Based Materials for Catalysis. *Catal. Sci. Technol.* **2012**, *2*, 54–75.
- (32) Malard, L. M.; Pimenta, M. A.; Dresselhaus, G.; Dresselhaus, M. S. Raman Spectroscopy in Graphene. *Phys. Rep.* **2009**, *473*, 51–87.
- (33) Petrie, W. T.; Vohs, J. M. Interaction of Platinum Films with the (0001) and (0001) Surfaces of ZnO. *J. Chem. Phys.* **1994**, *101*, 8098–8107.
- (34) Qiu, H.; Gallino, F.; Di Valentin, C.; Wang, Y. Shallow Donor States Induced by In-Diffused Cu in ZnO: A Combined HREELS and Hybrid DFT Study. *Phys. Rev. Lett.* **2011**, *106*, 066401.
- (35) Liu, Y.; Willis, R. F.; Emtsev, K. V.; Seyller, T. Plasmon Dispersion and Damping in Electrically Isolated Two-Dimensional Charge Sheets. *Phys. Rev. B* **2008**, *78*, 201403.

- (36) Koch, R. J.; Seyller, T.; Schaefer, J. A. Strong Phonon-Plasmon Coupled Modes in the Graphene/Silicon Carbide Heterosystem. *Phys. Rev. B* **2010**, *8*, 2201413.
- (37) Tanuma, S.; Powell, C. J.; Penn, D. R. Calculations of Electron Inelastic Mean Free Paths. V. Data for 14 Organic Compounds over the 50–2000 eV Range. *Surf. Interface Anal.* **1994**, *21*, 165–176.
- (38) Maki, H.; Ichinose, N.; Ohashi, N.; Haneda, H.; Tanaka, J. The Lattice Relaxation of ZnO Single Crystal (0001) Surface. *Surf. Sci.* **2000**, *457*, 377–382.
- (39) Lotya, M.; Hernandez, Y.; King, P. J.; Smith, R. J.; Nicolosi, V.; Karlsson, L. S.; Blighe, F. M.; De, S.; Wang, Z.; McGovern, I. T.; et al. Liquid Phase Production of Graphene by Exfoliation of Graphite in Surfactant/Water Solutions. *J. Am. Chem. Soc.* **2009**, *131*, 3611–3620.
- (40) Nemes-Incze, P.; Osváth, Z.; Kamarás, K.; Biró, L. P. Anomalies in Thickness Measurements of Graphene and Few Layer Graphite Crystals by Tapping Mode Atomic Force Microscopy. *Carbon* **2008**, *46*, 1435–1442.
- (41) Ferrari, A. C.; Meyer, J. C.; Scardaci, V.; Casiraghi, C.; Lazzeri, M.; Mauri, F.; Piscanec, S.; Jiang, D.; Novoselov, K. S.; Roth, S.; et al. Raman Spectrum of Graphene and Graphene Layers. *Phys. Rev. Lett.* **2006**, *97*, 187401.
- (42) Xu, K.; Cao, P.; Heath, J. R. Graphene Visualizes the First Water Adlayers on Mica at Ambient Conditions. *Science* **2010**, *329*, 1188–1191.
- (43) Law, Y. T.; Doh, W. H.; Luo, W.; Zafeiratos, S. A Comparative Study of Ethanol Reactivity over Ni, Co and NiCo-ZnO Model Catalysts. *J. Mol. Catal. A: Chem.* **2014**, *381*, 89–98.
- (44) Law, Y. T.; Skala, T.; Pis, I.; Nehasil, V.; Vondracek, M.; Zafeiratos, S. Bimetallic Nickel–Cobalt Nanosized Layers Supported on Polar ZnO Surfaces: Metal–Support Interaction and Alloy Effects Studied by Synchrotron Radiation X-ray Photoelectron Spectroscopy. *J. Phys. Chem. C* **2012**, *116*, 10048–10056.
- (45) Zafeiratos, S.; Dintzer, T.; Teschner, D.; Blume, R.; Haevecker, M.; Knop-Gericke, A.; Schloegl, R. Methanol Oxidation over Model Cobalt Catalysts: Influence of the Cobalt Oxidation State on the Reactivity. *J. Catal.* **2010**, *269*, 309–317.
- (46) Ha, D.-H.; Moreau, L. M.; Honrao, S.; Hennig, R. G.; Robinson, R. D. The Oxidation of Cobalt Nanoparticles into Kirkendall–Hollowed CoO and Co₃O₄: The Diffusion Mechanisms and Atomic Structural Transformations. *J. Phys. Chem. C* **2013**, *117*, 14303–14312.
- (47) Hyman, M. P.; Martono, E.; Vohs, J. M. Studies of the Structure and Interfacial Chemistry of Co Layers on ZnO(0001). *J. Phys. Chem. C* **2010**, *114*, 16892–16899.
- (48) Topsakal, M.; Şahin, H.; Ciraci, S. Graphene Coatings: An Efficient Protection from Oxidation. *Phys. Rev. B* **2012**, *85*, 155445.
- (49) Bunch, J. S.; Verbridge, S. S.; Alden, J. S.; van der Zande, A. M.; Parpia, J. M.; Craighead, H. G.; McEuen, P. L. Impermeable Atomic Membranes from Graphene Sheets. *Nano Lett.* **2008**, *8*, 2458–2462.
- (50) Venezia, A. M. X-ray Photoelectron Spectroscopy (XPS) for Catalysts Characterization. *Catal. Today* **2003**, *77*, 359–370.
- (51) Hess, C.; Tzolova-Mueller, G.; Herbert, R. The Influence of Water on the Dispersion of Vanadia Supported on Silica SBA-15: A Combined XPS and Raman Study. *J. Phys. Chem. C* **2007**, *111*, 9471–9479.
- (52) Martin, B. D.; Finke, R. G. Co–C Homolysis and Bond Dissociation Energy Studies of Biological Alkylcobalamins: Methyl-cobalamin, Including $\geq 10^{15}$ Co–CH₃ Homolysis Rate Enhancement at 25 °C Following One-Electron Reduction. *J. Am. Chem. Soc.* **1990**, *112*, 2419–2420.
- (53) Domenicano, A.; Hargittai, I. *Strength from Weakness: Structural Consequences of Weak Interactions in Molecules, Supramolecules, and Crystals*; Kluwer Academic Publishers: Dordrecht, The Netherlands, 2002.
- (54) Cancado, L. G.; Jorio, A.; Martins Ferreira, E. H.; Stavale, F.; Achete, C. A.; Capaz, R. B.; Moutinho, M. V. O.; Lombardo, A.; Kulmala, T. S.; Ferrari, A. C. Quantifying Defects in Graphene via Raman Spectroscopy at Different Excitation Energies. *Nano Lett.* **2011**, *11*, 3190–3196.
- (55) Wang, S.; Qiao, L.; Zhao, C.; Zhang, X.; Chen, J.; Tian, H.; Zheng, W.; Han, Z. A Growth Mechanism for Graphene Deposited on Polycrystalline Co Film by Plasma Enhanced Chemical Vapor Deposition. *New J. Chem.* **2013**, *37*, 1616–1622.
- (56) Eckmann, A.; Felten, A.; Mishchenko, A.; Britnell, L.; Krupke, R.; Novoselov, K. S.; Casiraghi, C. Probing the Nature of Defects in Graphene by Raman Spectroscopy. *Nano Lett.* **2012**, *12*, 3925–3930.
- (57) Blanc, N.; Jean, F.; Krasheninnikov, A. V.; Renaud, G.; Coraux, J. Strains Induced by Point Defects in Graphene on a Metal. *Phys. Rev. Lett.* **2013**, *111*, 085501.
- (58) Das, A.; Pisana, S.; Chakraborty, B.; Piscanec, S.; Saha, S. K.; Waghmare, U. V.; Novoselov, K. S.; Krishnamurthy, H. R.; Geim, A. K.; Ferrari, A. C.; et al. Monitoring Dopants by Raman Scattering in an Electrochemically Top-Gated Graphene Transistor. *Nat. Nanotechnol.* **2008**, *3*, 210–215.
- (59) Lee, J.; Novoselov, K. S.; Shin, H. S. Interaction between Metal and Graphene: Dependence on the Layer Number of Graphene. *ACS Nano* **2011**, *5*, 608–612.
- (60) Luo, Z.; Somers, L. A.; Dan, Y.; Ly, T.; Kybert, N. J.; Mele, E. J.; Johnson, A. T. C. Size-Selective Nanoparticle Growth on Few-Layer Graphene Films. *Nano Lett.* **2010**, *10*, 777–781.
- (61) Dahal, A.; Addou, R.; Croy-Diaz, H.; Lallo, J.; Batzill, M. Charge Doping of Graphene in Metal/Graphene/Dielectric Sandwich Structures Evaluated by C-1s Core Level Photoemission Spectroscopy. *APL Mater.* **2013**, *1*, 042107.
- (62) Zhang, L.; Ye, Y.; Cheng, D.; Pan, H.; Zhu, J. Intercalation of Li at the Graphene/Cu Interface. *J. Phys. Chem. C* **2013**, *117*, 9259–9265.
- (63) Haag, N.; Steil, S.; Großmann, N.; Fetzer, R.; Cinchetti, M.; Aeschlimann, M. Tailoring the Energy Level Alignment at the Co/Alq₃ Interface by Controlled Cobalt Oxidation. *Appl. Phys. Lett.* **2013**, *103*, 251603.
- (64) O'Hern, S. C.; Boutilier, M. S. H.; Idrobo, J.-C.; Song, Y.; Kong, J.; Laoui, T.; Atieh, M.; Karnik, R. Selective Ionic Transport through Tunable Subnanometer Pores in Single-Layer Graphene Membranes. *Nano Lett.* **2014**, *14*, 1234–1241.
- (65) Rubio-Marcos, F.; Calvino-Casilda, V.; Bañares, M. A.; Fernandez, J. F. Control of the Interphases Formation Degree in Co₃O₄/ZnO Catalysts. *ChemCatChem* **2013**, *5*, 1431–1440.
- (66) Koo, H.-M.; Lee, B. S.; Park, M.-J.; Moon, D.-J.; Roh, H.-S.; Bae, J. W. Fischer–Tropsch Synthesis on Cobalt/Al₂O₃-Modified SiC Catalysts: Effect of Cobalt–Alumina Interactions. *Catal. Sci. Technol.* **2014**, *4*, 343–351.
- (67) Gong, Y.; Meng, X.; Zou, C.; Yao, Y.; Fu, W.; Wang, M.; Yin, G.; Huang, Z.; Liao, X.; Chen, X. A Facile One-Pot Synthesis of Yolk–Shell ZnO Microsphere–Graphene Composite Induced by Graphene Oxide. *Mater. Lett.* **2013**, *106*, 171–174.